

From $\text{Ca}_{1-x}\text{Sm}_x\text{MnO}_3$ Synthesis to the Design and Characterization of Thermoelectric Module

Sébastien Lemonnier, Christophe Goupil, Emmanuel Guilmeau, Marlène Prevel, Jacques Noudem

Laboratoire CRISMAT, UMR CNRS ENSICAEN 6508
6 Bd Maréchal Juin, 14050 CAEN cedex
sebastien.lemonnier@ensicaen.fr

Abstract:

Since the discovery of the NaCo_2O_4 compound [1] with a large thermoelectric power S ($100\mu\text{V/K}$) and low resistivity ρ ($0.2\text{ m}\Omega\cdot\text{cm}$), a lot of efforts have been devoted to explore new oxides of high thermoelectric performance with the aim of device conception for energy conversion using Seebeck effect. As an example, the thermoelectric module [2] composed of *p*-type, $\text{Ca}_{2.7}\text{Bi}_{0.3}\text{Co}_4\text{O}_9$, and *n*-type, $\text{La}_{0.9}\text{Bi}_{0.1}\text{NiO}_3$, presents a high power output which confirms the potential of oxides in terms of energy conversion and the interest of their study. In this context Mn-based compounds CaMnO_3 perovskite are potential candidates for *n*-type materials in thermoelectric generators. These oxides are interesting due to their intrinsic transport properties ($S=-350\mu\text{V/K}$, $\rho=1\Omega\cdot\text{cm}$, at 300K) and also to the Mn mixed valence which allow a doping mechanism playing on carrier concentration and on their mobility [3, 4]. In this work, we present the complete building of an oxide thermoelectric generator from the optimization of $\text{Ca}_{1-x}\text{Sm}_x\text{MnO}_3$ compound based on, structural and electrical characterizations, to the design and characterization of the thermoelectric device.

KEYWORDS: *thermoelectric, Seebeck, module.*

1. Introduction

In a context of energy recovering and environmental protection, research in finding alternative energy source has led to potential thermoelectric applications. There are many applications of such devices where waste heat is produced, like in incinerators, factories, exhaust gas from cars... Moreover thermoelectric devices present many advantages since they are noiseless, they do not require any movable mechanical parts and they are highly reliable. The discovery of thermoelectric oxide with good performances, like CoO_2 -based oxides [5-7] has allowed building thermoelectric modules that can work in a larger range of temperature than typical metal-based devices, with hot temperature close to 1000K . Such high temperatures imply that fabrication is really different than for conventional thermoelectric modules, in particular in the way to link thermoelectric bars between us. For that purpose we describe the synthesis of $\text{Ca}_{0.95}\text{Sm}_{0.05}\text{MnO}_3$ compound, and discuss about the influence of sintering temperature and densification type, on thermoelectric properties. Mn-based oxide bars have then been integrated in a four-leg thermoelectric device which has been fully characterized in term of thermal and electrical properties.

2. Compounds

a) Experimental

Polycrystalline samples of $\text{Ca}_{0.95}\text{Sm}_{0.05}\text{MnO}_3$ were synthesized by solid state reaction in air. The precursors CaCO_3 , MnO_2 and Sm_2O_3 were mixed in stoichiometric proportions and powder was first calcinated at 900°C for 24 hours.

In order to observe the influence of pressure type, two pairs of samples were prepared, the firsts using uniaxial pressure, and the second one using isostatic press (3 tons). For each type of samples two sintering temperature were investigated, 1350°C and 1450°C (2 hours), in order to evidence the influence on thermoelectric properties. The samples and processing conditions are presented [table 1](#). One can notice that the electrical resistivity ρ ($\text{m}\Omega\cdot\text{cm}$) strongly depends of numerous factors, like material's density, contrary to Seebeck coefficient S ($\mu\text{V/K}$) which only depends of phase composition. Increasing densification, pressure and sintering temperature could then allow a decrease of ρ without any modification of S . Higher values of the power factor $P = S^2/\rho$ ($\text{W/K}^2\text{m}$) are expected using this two methods. Powders purity was systematically checked by XRD patterns using the $\text{CuK}\alpha$ radiation of a X'Pert pro diffractometer. Samples microstructures were observed by SEM on a Supra55 Zeiss, and EDS analysis were used to check grains composition.

At low temperature, resistivity measurements were performed on PPMS (Physical properties measurement system) from Quantum Design using

the standard DC four-probe method and Seebeck coefficient measurements were carried out on a PPMS-based system. At high temperature, resistivity and Seebeck coefficient measurements were investigated using a ZEM-3 apparatus (ULVAC).

For low temperature measurements, contacts were glued using Ag-paste (4929N, Dupont) and annealed at 920°C for 2 hours. At high temperature, with ZEM-3 apparatus, only mechanical contacts are needed, by pressing thermocouples on samples side.

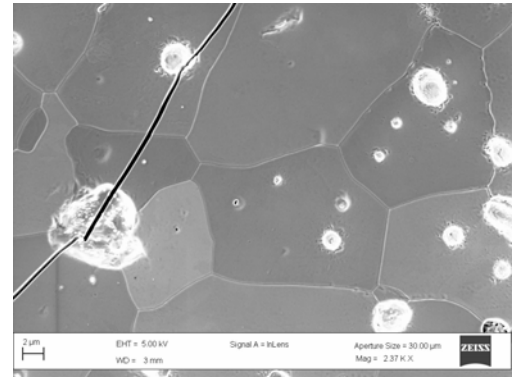


Figure 2: Micrography of a polished and quenched $\text{Ca}_{0.95}\text{Sm}_{0.05}\text{MnO}_3$ compound

composition	$\text{Ca}_{0.95}\text{Sm}_{0.05}\text{MnO}_3$	$\text{Ca}_{0.95}\text{Sm}_{0.05}\text{MnO}_3$	$\text{Ca}_{0.95}\text{Sm}_{0.05}\text{MnO}_3$	$\text{Ca}_{0.95}\text{Sm}_{0.05}\text{MnO}_3$
number	1	2	3	4
Heat treatment	1350°C	3t + 1350°C	1450°C	3t + 1450°C

Table 1: Composition and heat treatment for the studied compounds

b) Results and discussion

The XRD patterns reported [figure 1](#), indicate that all the samples are single phase and the high definition of peaks, like the 220 peak diffraction at 34° or the 400 peak at 49° shows that samples are well crystallized. The absence of extra peaks confirms that no secondary phases are present. So the Samarium has really taken the Calcium's site in the structure and the EDS analyses confirm the nominal cationic composition. Micrography of a $\text{Ca}_{0.95}\text{Sm}_{0.05}\text{MnO}_3$ sample, densified by isostatic press and sintered at 1450°C is presented [figure 2](#). In order to reveal grain boundaries, the sample was polished and quenched at 1200°C for 3 minutes. The average grain size is about few micrometers and no secondary phases are observed. (The crack visible on micrography is due to the thermal shock during the quench).

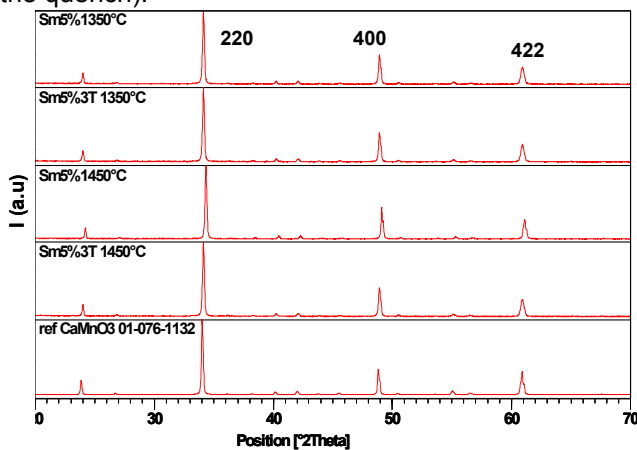


Figure 1: XRD patterns. From top to bottom: samples 1,2,3,4 and CaMnO3 reference.

The influence of sintering temperature on ρ is presented [figure 3](#). The two samples present semiconductor behaviour at low and intermediate temperatures. As expected a decrease of the resistivity values is observed when increasing the sintering temperature from 1350°C to 1450°C. Values of ρ at 300K are respectively 5.8 and 4.8 mΩ.cm and at 800K 12 and 8.6 mΩ.cm. This can be correlated with the increase of relative density from 70 to 80 % of the theoretical density using isostatic press.

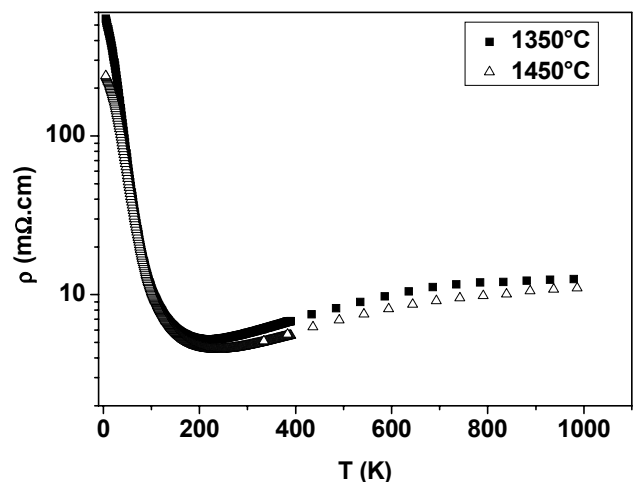


Figure 3: Influence of sintering temperature on electrical resistivity

The influence of type of pressing and pressure on electrical resistivity is illustrated [figure 4](#). The samples 3 and 4 both processed at 1450°C were

performed since they present lower electrical resistivity values than those sintered at 1350°C. One can see that the two samples present the same semiconductor behaviour at low temperature which turns into metallic behaviour at higher temperature. The electrical resistivity is lower for the samples densified using isostatic press as predicted. This is coherent with the increase of density from 80 to 90 % of the theoretical density. The values for the best sample (isostatic press and sintering at 1450°C) at 300K and 800K are respectively 3.7 and 7.6 mΩ.cm. Figure 5 presents the temperature dependence of the Seebeck coefficient for the sample 4. One can notice the good agreement between measurements obtained by the two apparatus. The Seebeck values for 300K and 800K are respectively -150 and -198 μV/K.

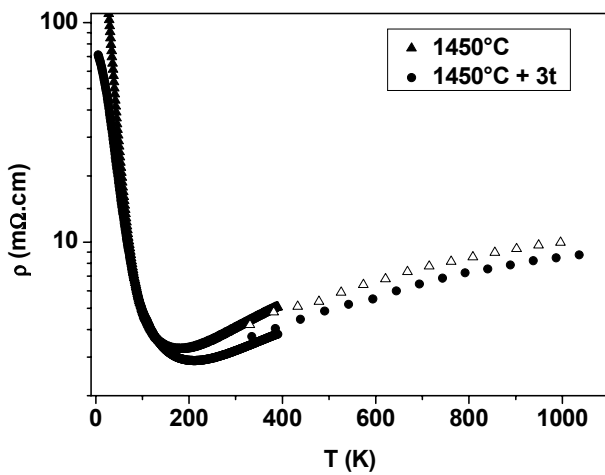


Figure 4: Influence of densification type and pressure on electrical resistivity

These methods allow to increase the power factor defined as $P=S^2\rho$ (W/K²m) where S (μV/K) is the Seebeck coefficient and ρ (mΩ.cm) the electrical resistivity. The calculated power factors reach 0.61 mW/K²m at 300K and 0.51 mW/K²m at 800K. These values are higher than those obtained until now on CaMn_{0.96}Nb_{0.04}MnO₃ (0.3 mW/K²m) and Ca_{0.9}Bi_{0.1}MnO₃ (0.27 mW/K²m) [8-10]. The electrical values at room temperature of all samples are presented table 2.

Heat treatment	1350°C	3t + 1350°C	1450°C	3t + 1450°C
Sample	1	2	3	4
ρ (mΩ.cm) 300K	5.8	5.3	4.8	3.7

Table 2: Electrical resistivity of the four samples at 300K

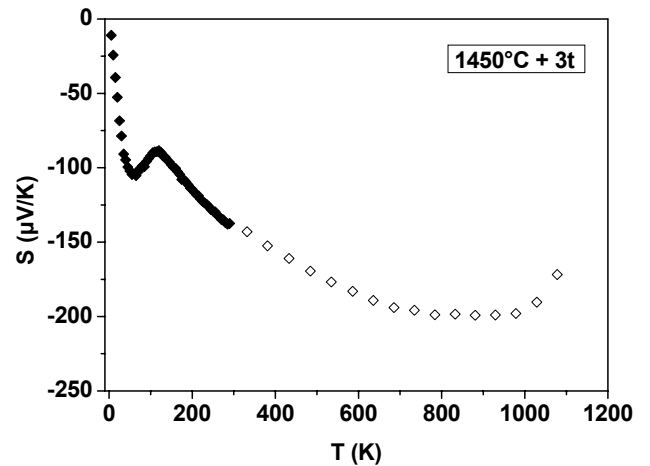


Figure 5: Seebeck coefficient of the Ca_{0.95}Sm_{0.05}MnO₃ compound versus temperature

3. Thermoelectric device and characterizations

a) Module fabrication

According to the results obtained on the Ca_{0.95}Sm_{0.05}MnO₃ compounds, the material pressed by isostatic press at 3t and sintered at 1450°C for 2 hours has been integrated as a n-type material in a four legs oxide module. The well known Ca₃Co₄O₉ compound [4] synthesized using isostatic press at 3t, at 920°C for 24h, has been integrated in the device as p-type material. The fabrication process is separated in three parts:

- synthesis and shaping of oxide legs
- fitting of bars between alumina plates using silver stripes and paste
- annealing of the all device.

The synthesis step for the Ca_{0.95}Sm_{0.05}MnO₃ has been presented in the first part. For the p-type material, the Co-based oxide was synthesized from stoichiometric amounts of CaCO₃ and Co₃O₄, by solid state reaction. The precursor powder was mixed and calcinated for 24 h at 900°C. The mixture powder was first shaped into cylindrical bars using isostatic press at 3t and was sintered at 920°C for 24 hours according to the Ca-Co-O phase diagram. The obtained samples were cut as bars of 5mm length and 6mm diameter in order to have 4 legs of the same dimensions.

Bars are placed electrically in series and thermally in parallel and joined by silver stripes of 1mm thick. The silver stripes are stocked between alumina plates, of 25*25mm² and 1.5 mm thick, and bars using silver paste (2949N from Dupont).

The assembled module is placed in a furnace and annealed at 920°C for 12 hours in order to obtain good electrical and thermal contacts. Figure 6 presents the thermoelectric device before this heat treatment.

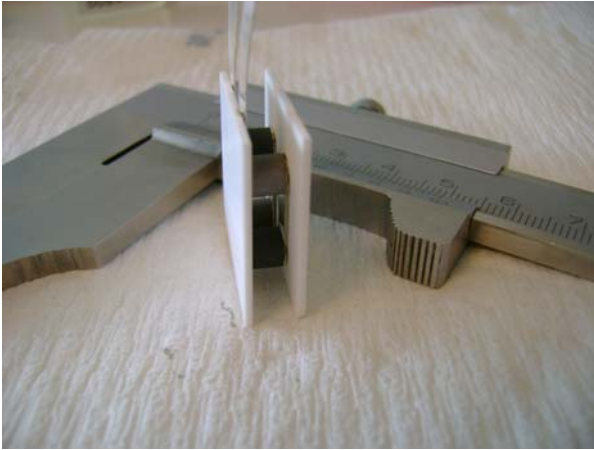


Figure 6: Four legs oxide thermoelectric device before annealing

b) Module evaluation and results

A home made apparatus has been designed to evaluate thermoelectric modules performances. Temperature difference of up to $\Delta T = T_{hot} - T_{cold} = 500^\circ\text{C}$ along the length of oxide bars can be created by heating the top alumina plate using mica heater embedded in copper plates. The bottom plate alumina is maintained near the room temperature using a copper block cooled by water circulation. The operation of the module is recorded in order to measure simultaneously the thermal and electrical parameters using Keithley 2700 scanning system. Measurements were done with different loads (from 0 to 2.2Ω in this case) on the device in order to obtain all the parameters in open, close (and short) circuit modes. In open circuit mode, $T_{hot \text{ module}}$, $T_{cold \text{ module}}$, $T_{hot \text{ leg p}}$, $T_{cold \text{ leg p}}$, $T_{hot \text{ leg n}}$, $T_{cold \text{ leg n}}$, ΔV_p , ΔV_n and E_0 can be measured and registered using k type thermocouples (figures 7 and 8). The short circuit measurement allows estimating the electrical resistance of load wires and contacts. Then the measurements with varied load resistances allow the extraction of the internal resistance R_{in} . By the relation $I_{out} = E_0 / (R_{load} + R_{in})$ it is then possible to calculate the internal module resistance and so the electrical contact resistance. Since, ΔV_p and ΔV_n are measured, along p and n bars, $R_{p \text{ bar}}$ and $R_{n \text{ bar}}$ can be calculated. Then the resistivities of the two materials can be extracted as $\rho_p = R_{p \text{ bar}} * S / l$ and $\rho_n = R_{n \text{ bar}} * S / l$ where R is the bar resistance measured, S the section of bar and l the distance between contacts.

E_0 is directly given by the sum of thermoelectric voltage contributions and R_{in} by the thermoelectric materials resistance contribution. In practice, contact resistances are not negligible and R_{in} corresponds to the sum of the two terms. A manufacturing factor which traduces the quality of a

thermoelectric module can be calculated considering the ratio $M.F = R_{in \text{ ideal}} / R_{in}$.

The performance of this module were finally checked three times, at $t=0$, $t=50\text{h}$ and $t=100\text{h}$ with intermediate cycle of 1h for the rises and the descents and 6h of stage with T_{hot} near of 600°C . These measurements give first insight of the reliability.

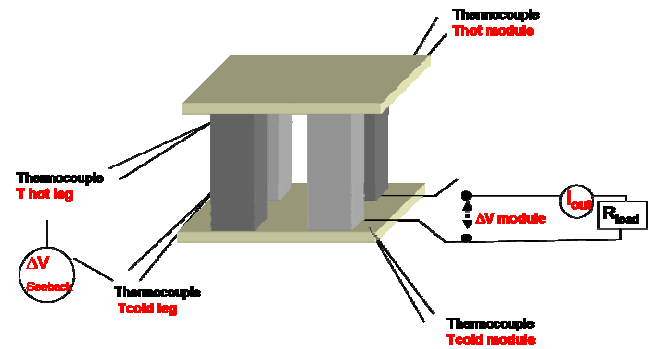


Figure 7: Thermoelectric device measurement system

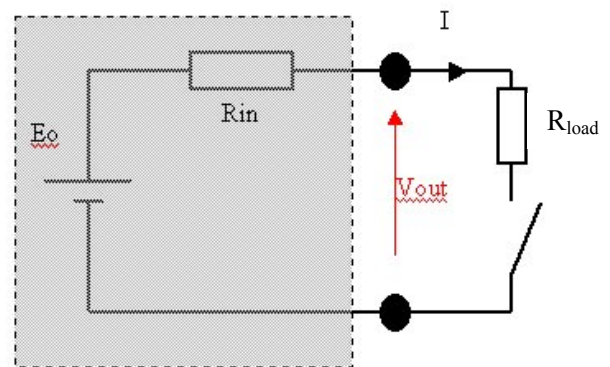


Figure 8: electrical equivalent of a thermoelectric module (grey)

The average Seebeck voltage normalized by the temperature difference was directly measured in open circuit mode on the device. The values of Seebeck coefficient obtained for each type of compound, are presented figure 9, in function of $\langle T \rangle = T_{hot \text{ module}} - T_{cold \text{ module}}$ along the bar. There is a good agreement with measurement carried out on ZEM-3 apparatus for the n-type. Considering the previous results reported for the Co-based compound, values obtained are slightly lower in our case [11, 12, and 13].

The figure 10 presents the E_0 experimental values obtained and the E_0 theoretical values calculated using the relation:

$$E_{0 \text{ theo}} = 2 * (S_p - S_n) * \Delta T_{module}$$

One can see the excellent agreement between theoretical and experimental values.

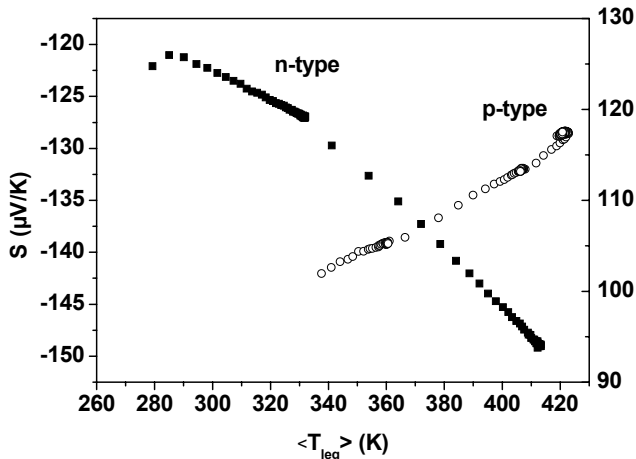


Figure 9: Seebeck coefficient for each p-type and n-type in function of average temperature along the bar

The measurement with different load resistance values, R_{load} , from open circuit ($R_{load} \infty$ to 2.2Ω in our case) allows extracting the contact resistance values, using the relations:

$$V_{out} = E_0 \frac{R_{load}}{R_{in} + R_{load}}$$

$$I_{out} = \frac{E_0}{R_{in} + R_{load}}$$

$$V_{out} = E_0 - R_{in} I_{out}$$

The plot of V_{out} versus I_{out} gives a linear plot with a slope equals to R_{in} and origin ordinate equals to E_0 . As previously said the internal resistance contains both material and contact resistance contributions $R_{contact}$. This latter can then be easily extracted. Figure 11 presents the V_{out} measured in function of I_{out} for the different load resistances. R_{in} present a value of $341 \text{ m}\Omega$ and E_0 reaches -162 mV at $T_{hot} = 650\text{K}$ and $\Delta T_{module} = 320\text{K}$.

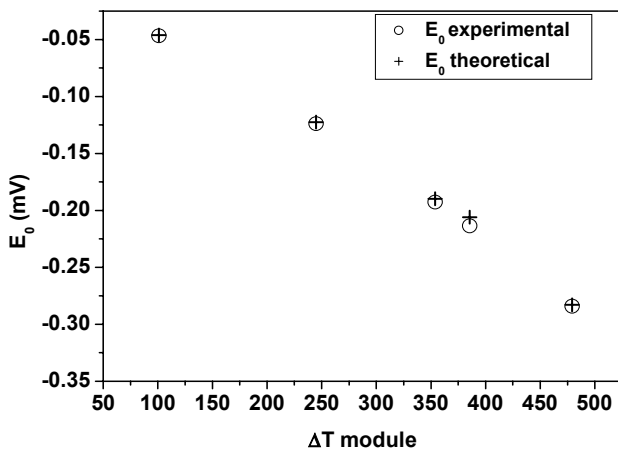


Figure 10: Experimental and theoretical values of E_0 for the thermoelectric device

The manufacturing factor for this thermoelectric device is 26% ($M.F = R_{in-ideal} / R_{in}$). It is important to

note that smaller is the leg size module larger is the influence of contact resistance value in device internal resistance. The measurements, not presented here, after several cycles of 7 hours, carried out at $t=50\text{h}$ and $t=100\text{h}$ have shown no deterioration within the thermoelectric device.

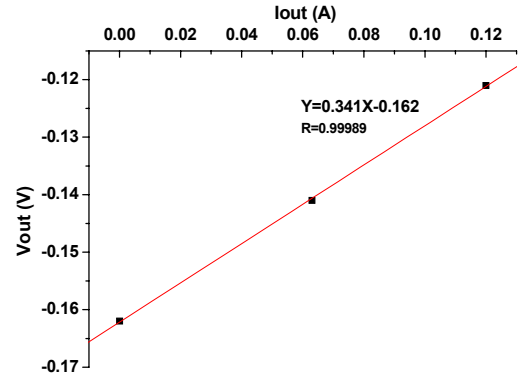


Figure 11: V_{out} versus I_{out} for the thermoelectric device

4. Conclusion

In conclusion, it has been shown that improvement of thermoelectric properties is possible increasing material's density by two methods: the increase of sintering temperature and the use of isostatic press. The power factor of the $\text{Ca}_{0.95}\text{Sm}_{0.05}\text{MnO}_3$ compound reaches $0.61 \text{ mW/K}^2\text{m}$ at 300K and $0.51 \text{ mW/K}^2\text{m}$ at 800K .

A manufacturing factor of 26% has been obtained, revealing efforts still have to be made in order to reduce contact resistance.

References

- [1] I. Terasaki, Y. Sasago, and K. Uchinokura, Phys. Rev. B 56, R12685 (1997)
- [2] R. Funahashi, S. Urata, K. Mizuno, T. Kouuchi, and M. Mikami, Appl. Phys. Lett., 85, 1036 (2004); R. Funahashi, M. Mikami, T. Mihara, S. Urata, and N. Ando, J. Appl. Phys. 99, 066117 (2006)
- [3] Urushibara, A. Moritomo, Y. Arima, T. Asamitsu, A. Kido, G. Tokura, Y. Phys. Rev. B 51, 14103 (1995)
- [4] Rao, C.N.R.; Cheetham, A.K.; Mahesh, R. Chem. Mater 8, 2421 (1996)
- [5] R. Funahashi, I. Matsubara, H. Ikuta, T. Takeuchi, U. Mizutani, and S. Sodeoka, Jpn. J. Appl. Phys., Part 2 39, L1127 (2000).
- [6] R. Funahashi and I. Matsubara, Appl. Phys. Lett. 79, 362 (2001).
- [7] A.C. Masset, C. Michel, A. Maignan, M. Hervieu, O. Toulemonde, F. Studer, B. Raveau and J. Hejtmanek : Physical Review B 62, 166 (2000)
- [8] Gaojie Xu, Ryoji Funahashi, Ichiro Matsubara and Masahiro Shikano and Yuqin Zhou : J. Mater. Res. 17, 1092-1095 (2002)
- [9] Michitaka Ohtaki, Hisako Koga, Tsutomu Tokunaga, Koichi Eguchi and Hiromichi Arai : Journal of Solid State Chemistry, Volume 120, Issue 1, 15 November 1995, Pages 105-111
- [10] T. Kobayashi, H. Takizawa, T. Endo, T. Sato, M. Shimada, H. Taguchi and M. Nagao : Journal of Solid State Chemistry, Volume 92, Issue 1, May 1991, Pages 116-129
- [11] Kazuyoshi Suzuki, Hiroyuki Fujishiro, Yohei Kashiwada, Yosuke Fujine and Manabu Physica B: Physics of Condensed Matter, Volume 329, p. 922-923.
- [12] Yuzuru Miyazaki Solid State Ionics 172 (2004) 463-467
- [13] J. Hejtmanek, Z. Jirák, and M. Maryško
C. Martin, A. Maignan, M. Hervieu, and B. Raveau Phys. Rev. B 60, 14057 - 14065 [Issue 20 - November 1999]